Optimizing the multicycle subrotational internal cooling of diatomic molecules

A. Aroch,[1] S. Kallush,[1,2] and R. Kosloff[1]

[1]*The Fritz Haber Research Center, The Hebrew University of Jerusalem, Jerusalem 91904, Israel*

[2]*Department of Physics and Optical Engineering, ORT-Braude College, P.O. Box 78, 21982 Karmiel, Israel*

(Received 12 February 2018; published 10 May 2018)

Subrotational cooling of the AlH^+ ion to the miliKelvin regime, using optimally shaped pulses, is computed. The coherent electromagnetic fields induce purity-conserved transformations and do not change the sample temperature. A decrease in a sample temperature, manifested by an increase of purity, is achieved by the complementary uncontrolled spontaneous emission which changes the entropy of the system. We employ optimal control theory to find a pulse that stirs the system into a population configuration that will result in cooling, upon multicycle excitation-emission steps. The obtained optimal transformation was shown capable to cool molecular ions to the subkelvins regime.

DOI: 10.1103/PhysRevA.97.053405

I. INTRODUCTION

Ultracold molecules are a new form of matter with unique quantum properties [1]. The additional internal structure, for example, their dipole moments, will determine their collective properties [2]. The promise of new physics has initiated a quest to trap and cool molecules to their quantum degeneracy [3,4]. Experiments that aim to approach such a state of matter in the ground state of the molecule are now at the focus of several groups. The difficulty stems from the additional requirement of also cooling the internal degrees of freedom, vibration, and rotation, and fine and hyperfine structure.

Two general directions have been followed to obtain ultracold neutral molecules: (i) Direct trapping and cooling of stable molecules. Typically the first step is stopping and trapping the molecules, followed by additional cooling of internal degrees of freedom [5]. These methods include buffer gas cooling [6], sympathetic cooling [7], and field manipulation (radiative cooling) [8,9]. (ii) Indirect methods that assemble ultracold molecules from ultracold atomic species. The most studied method employs photoassociation from free atoms [10] or enhancing the process via a Feshbach resonance [11]. The typical trap depth of molecules, which serve as the starting point for the internal cooling which is further needed in order to approach quantum degeneracy, is of the order of hundreds of miliKelvins [12].

Molecular ions are relatively easy to isolate and trap spatially due to their strong Coulombic interactions, but are more difficult to cool internally. The initial temperatures for the internal cooling for ions are thus much higher and could even reach room temperature.

The present study is devoted to the study of cooling internal degrees of freedom of trapped ionic molecules. In analogy with laser cooling of atoms, a sequential laser cooling of vibration and rotation based on narrowband lasers was suggested, addressing all transitions [13]. As an alternative to this complicated comb spectrum, one can imagine a broadband spectrum where the unwanted transitions are removed. This alternative cooling scheme was suggested based on a shaped broadband sequence of pulses followed by spontaneous emission [14]. Optimal control theory was used to find the required pulse shape [15,16]. Analyzing the cooling mechanism revealed that the target state became a dark state to the excitation pulse, thus optically pumping all other states. This idea was realized experimentally for vibrational cooling of photoassociated cesium molecules [17]. The experimental success inspired additional studies of broadband cooling [18,19].

Cooling rotational degrees of freedom is a more difficult task due to smaller energy spacings and a large number of available states [19]. Nevertheless, for hydrides with a relatively large rotational spacing, carefully shaped broadband excitations can lead to cooling [20].

A recent experimental study [20] demonstrated rotational cooling to the ground rotational level $J = 1/2$ of AlH^+ by filtered broadband excitation. For this molecular ion, the excitation from the $X^2\Sigma$ ground electronic state to the first excited $A^2\Pi$ state resulted in a minimal modification of the electronic internuclear potential. Under these conditions, the Franck-Condon (FC) factors which determine the branching of a vibrational state during the excitation and emission eliminate practically all the transitions between states with different vibrational quantum number v (see Fig. 1). Despite its experimental robustness, the filtered broadband method is limited by the resolution of the applied filter, and hence subrotational cooling is difficult. The cooling is slow (140 ms) so that $\sim 10^6$ cycles of excitation relaxation are needed to reach a steady-state temperature of $T \sim 4$ K (see Fig. 1).

The present theoretical study is aimed at exploring schemes to enhance the cooling rate of AlH^+ and reach a lower target temperature. We will employ optimal control theory to find broadband-shaped pulses that can enhance the rotational cooling.

The paper is arranged as follows: Section II presents the model for the light-matter interaction framework. Section III describes the theoretical tools that are used for achieving control. Section IV presents the results, which are discussed and summarized in the concluding Sec. V.

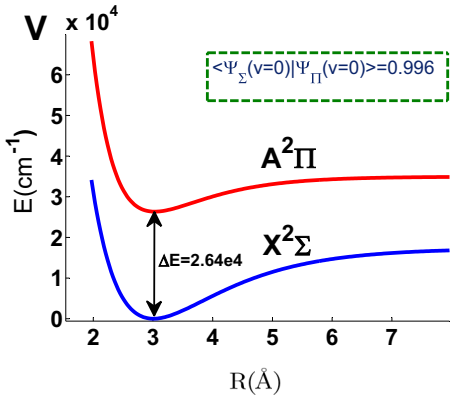

FIG. 1. Electronic potential curves for AlH^+. The $X^2\Sigma$, $A^2\Pi$ potentials are displayed and, in addition, the FC factors between the ground vibrational state of the two electronic states is presented.

II. THE LIGHT-MATTER INTERACTION MODEL

To model the full dynamics of the molecule on two electronic surfaces, the state of the systems is described by the combined density operator,

$$\hat{\rho} = \hat{\rho}_g \otimes \hat{P}_g + \hat{\rho}_e \otimes \hat{P}_e + \hat{\rho}_c \otimes \hat{S}_+ + \hat{\rho}_c^* \otimes \hat{S}_-, \quad (1)$$

where $P_{g/e}$ are the projection operators of the ground and excited electronic state, $\hat{S}_{+/-}$ are the electronic raising and lowering operators, $\rho_{g/e}$ are the density operator for the rovibrational ensemble within the ground and excited electronic states, and ρ_c is the density operator of the nuclear coherence between the surfaces. The Hamiltonian of such a system is

$$\begin{aligned} \hat{H} &= \hat{H}_0 + \hat{V}_t, \\ \hat{H}_0 &= \hat{H}_g \otimes \hat{P}_g + \hat{H}_e \otimes \hat{P}_e, \end{aligned} \quad (2)$$

where $\hat{H}_{g/e}$ is the ground and excited rotational Hamiltonian. The interaction of the system with light is described by $\hat{V}_t$,

$$\hat{V}_t = -\sum_{q=X,Y,Z} \hat{\mu}_q \otimes (\hat{S}_+ \varepsilon_q + \hat{S}_- \varepsilon_q^*), \quad (3)$$

where $\hat{\mu}_q$ is the transition dipole moment along the q spatial direction and $\varepsilon_q(t)$ represents the time-dependent field along the same direction.

$\hat{H}_{g/e}$ are the field-free rovibrational Hamiltonians. For mildly cold temperatures ($T_{\text{initial}} \leqslant 20$ K) and high vibrational frequency, we can assume that the molecules are initially in their ground $v = 0$ state. Moreover, vibrational excitations in the electronic transition are negligible due to the highly restricting FC factors [20]. As a result, the modeling is thus restricted to $v = 0$.

The rotational states of the model are expanded by the symmetric top basis [21],

$$|J\Omega M\rangle = \left[\frac{2J+1}{4\pi}\right]^{\frac{1}{2}} D^J_{M\Omega}(\phi,\theta,0), \quad (4)$$

where J is the total molecular angular momentum, and M and Ω are its projections on the spatial (Z) and molecular (z) axis, respectively. Here, $D^J_{M\Omega}$ is the rotational tensor.

For the ground electronic $^2\Sigma$ state, the projection of the spatial electronic angular momentum on the molecular axis $\Lambda = 0$ and the electronic spin is $S = \frac{1}{2}$ (so $\Sigma = \pm\frac{1}{2}$, the projection of S on an internuclear axis), and Hund's case (b) is applicable. The molecular energy eigenfunctions become

$$\begin{aligned} |gJ\Omega M\pm\rangle = \frac{1}{\sqrt{2}}\Bigg[&\left|S=\frac{1}{2},\Sigma=\frac{1}{2}\right\rangle|J\Omega M\rangle \\ &\pm\left|S=\frac{1}{2},\Sigma=-\frac{1}{2}\right\rangle|J-\Omega M\rangle\Bigg], \end{aligned} \quad (5)$$

where $\pm$ denotes the sign of the linear combination and is related to the parity of the wave function. The rotational energies for each of the parities are given by

$$\begin{aligned} E_g^1(J) &= B_g\left(J-\tfrac{1}{2}\right)\left(J+\tfrac{1}{2}\right) + {}^1\!/_2\gamma_g\left(J-\tfrac{1}{2}\right), \\ E_g^2(J) &= B_g\left[\left(J+\tfrac{1}{2}\right)\left(J+\tfrac{3}{2}\right)\right] - {}^1\!/_2\gamma_g\left(J+\tfrac{3}{2}\right), \end{aligned} \quad (6)$$

where $E_g^1(J)$ and $E_g^2(J)$ denote the F_1 and F_2 manifolds described by [21]. $B_g = 6.76$ cm^{-1} is the rotational constant for the ground vibrational state, $\gamma_g = 5.66\times10^{-2}$ cm^{-1} is the spin-*nuclear* rotation constant, and $J = \frac{1}{2},\frac{3}{2},\frac{5}{2},\ldots$.

In the excited $^2\Pi$ state, $\Lambda = \pm1$ and $\Omega = -\frac{3}{2}, -\frac{1}{2}, \frac{1}{2}, \frac{3}{2}$. This state is an intermediate between Hund's case (a) and case (b), where L is coupled to the internuclear axis and S is uncoupled from the nuclear axis. Each (J,M) level has four rotational levels associated with it, two of each parity:

$$\begin{aligned} |J|\Omega|M\pm\rangle = \frac{1}{\sqrt{2}}[&|\Lambda=1\rangle\left|\frac{1}{2}\frac{1}{2}\right\rangle|J+\Omega M\rangle \\ &\pm|\Lambda=-1\rangle\left|\frac{1}{2}-\frac{1}{2}\right\rangle|J-\Omega M\rangle]. \end{aligned} \quad (7)$$

The energies are given by

$$\begin{aligned} E_e^{\pm}(J) &= B_e\left[\left(J-{}^1\!/_2\right)\left(J+{}^3\!/_2\right) \pm {}^1\!/_2X\right], \\ X &= \sqrt{\left[4\left(J-{}^1\!/_2\right)\left(J+{}^3\!/_2\right)+(Y-2)\right]}, \\ Y &= \frac{A_e}{B_e}. \end{aligned} \quad (8)$$

$B_e = 6.85$ cm^{-1} is the rotational constant for the excited electronic state, and $A_e = 106$ cm^{-1} is the spin-*electronic* orbital coupling.

The $\pm X$ assigns the corresponding eigenvectors,

$$|eJM+\rangle = a_j\left|J^1\!/_2M\right\rangle + b_j\left|J^3\!/_2M\right\rangle \quad (9)$$

and

$$|eJM-\rangle = -b_j\left|J^1\!/_2M\right\rangle + a_j\left|J^3\!/_2M\right\rangle, \quad (10)$$

where

$$\begin{aligned} a_j &= \left[\frac{X+(Y-2)}{2X}\right]^{\frac{1}{2}}, \\ b_j &= \left[\frac{X-(Y-2)}{2X}\right]^{\frac{1}{2}}. \end{aligned} \quad (11)$$

The additional energy split by the coupling of the molecular magnetic moment and the nuclear rotation is small enough and

has been neglected here. That is, hyperfine cooling will not be considered within this framework.

The transitions between the two electronic states $^2\Sigma \rightarrow {}^2\Pi$ are dictated by dipole selection rules ($\Delta J = 0, \pm 1$), denoted as R, Q, and P branches, respectively. The coupling elements can be found by calculating the overlap of any two eigenvectors with the dipole operator.

At thermal equilibrium, the initial state ρ_{eq} is characterized by thermally distributed populations in the quantum states,

$$\hat{\rho}_{eq} = \frac{1}{Z}\sum_j e^{-\beta E_g^{\pm}(j)} |g\,J\,M\pm\rangle\langle g\,J\,M\pm|, \tag{12}$$

where $\beta = 1/k_bT$ and the sets $|J\Omega M\pm\rangle$ and $\{E_i\}$ are the eigenstates and eigenenergies of the system, and Z is the partition function.

For the AlH^+ at the temperature of 5 K, close to the final temperature in [20], less than 0.01 of the population occupies $J > \frac{1}{2}$ and only four states are thermally populated. In the present study, we assume an initial temperature of 20 K, which restricts the population occupation up to $J = \frac{3}{2}$ states (12 states).

The evolution of the system will be governed by the Liouville–von Neumann equation [22]

$$\frac{d\hat{\rho}}{dt} = -\frac{i}{\hbar}[\hat{H},\hat{\rho}] + L_D(\hat{\rho}), \tag{13}$$

where the first term is the coherent dynamical part governed by the Hamiltonian and the second term is the dissipative part of the dynamics governed by the Liouvillian superoperator. This equation represents the dynamics of an open quantum system.

For optical transitions with multiple pulses, there is a distinct timescale separation between the light-induced step which occurs in less than a picosecond and is unitary, the incoherent decay which occurs in tens of nanoseconds, and the pulse repetition rate which is in the MHz to KHz range. Within this picture, each cooling cycle could be separated into two parts: (1) The short-time interaction of the external field and the molecular system. Since this step is unitary, the density operator can be decomposed to energy eigenstates and each component can be computed in a wave-function framework. Then, (2) a slow and field-free spontaneous decay takes place. In this step, the coherences developed between energy eigenstates during the laser-controlled step are erased. The probability of transformation from a given excited-state energy eigenstate to the ground-state manifold of states is dictated by Fermi's golden rule,

$$\Gamma_{i\rightarrow f} \approx \sum_q |\langle e\,J\,M\pm|\hat{\mu}_q|g\,J\,M\pm\rangle|^2. \tag{14}$$

Note that while the former coherent step yields only unitary transformations and therefore does not change the purity, the latter decay step is a unidirectional positive map which does not maintain the purity and thus change the temperature of the system.

The final nonequilibrium steady state of the system does not have to be thermal. To associate an effective temperature to the state, we employ the von Neumann entropy to scale the purity and, consequently, define the effective temperature. The idea came from information theory where the entropy is related to the probability distribution of an ensemble [22]. The entropy is defined as

$$S_{VN} = -\mathrm{tr}\{\hat{\rho}\ln\hat{\rho}\} \leqslant -\sum_j P_j \ln P_j, \tag{15}$$

where ρ is the density matrix of the system and P_j is the probability to be in the energy eigenstate j, which is the only contribution to the entropy, under the assumption that quantum coherences do not survive the spontaneous-emission incoherent step. Equality will be obtained when the system is diagonalized in the energy domain. It is important to note that entropy is invariant under unitary transformation, and therefore any steady state reached after cooling can be transformed by unitary transformation to a passive state with the same entropy [23]. To define a temperature of any nonthermal state, we associate it with the temperature of a thermal state with the same von Neumann (vN) entropy.

III. CONTROLLING THE SYSTEM

Quantum optimal control theory (OCT) is a branch of coherent control, a quantum-mechanical-based method for controlling dynamical processes. The basic principle is to control quantum interference phenomena typically by shaping the phase of laser pulses [24–27]. OCT is formulated as a maximization problem and seeks a time-dependent field that maximizes the expectation value of an operator in final time.

Consider a quantum system in an initial state $\hat{\rho}_0 = \sum_{k=1}^{n} p_k|\psi_k^0\rangle\langle\psi_k^0|$, where the set $\{\psi_k^0\}$ is energy eigenstates of the system. The control will seek a field that maximizes the expectation value of the operator $\hat{O}$ at final time T,

$$J_{\max}(\varepsilon) \equiv \sum_{k=1}^{n} p_k\langle\Psi_k(T)|\hat{O}|\Psi_k(T)\rangle, \tag{16}$$

where $\Psi_i(T)$ describes the state that results from the interaction of the system with the field,

$$\vec{\varepsilon}(t) = \sum_q \varepsilon_q(t)\hat{q}, \tag{17}$$

at the final time T. Here, $\hat{q}$ are spatial directions. The governing of the dynamics of the system by the Schrödinger equation $i\frac{\partial}{\partial t}|\psi\rangle = \hat{H}|\psi\rangle$, with the Hamiltonian

$$\hat{H}(t) = \hat{H}_0 - \vec{\mu}\cdot\vec{\epsilon}(t), \tag{18}$$

is enforced by adding an additional cost term to the functional, according to the Lagrange-multiplier method,

$$J_{\mathrm{con}} = \sum_{k=1}^{n} -2\mathrm{Re}\int_0^T \langle\chi_k(t)|\frac{d}{dt} + i\hat{H}(t)|\psi_k(t)\rangle dt, \tag{19}$$

where $\{\langle\chi_k(t)|\}$ are the set of time-dependent Lagrange multipliers.

To regularize the solution with a limitation over the intensity, another penalty term to the functional is added [28],

$$J_{\mathrm{penal}}(\varepsilon) = -\sum_q \alpha_q \int_0^T \varepsilon_q^2(t)dt, \tag{20}$$

where α_q are scalar Lagrange multipliers. The overall object of maximization is the following functional:

$$J = J_{\max} + J_{\text{penal}} + J_{\text{con}}. \tag{21}$$

The maximization of the fitness J is the control task. Functional derivatives with respect to the various field and wave-function components are then taken, resulting in the following system of equations (22) and (23).

Each of the set of the $|\chi_k(t)\rangle$ Lagrange multipliers will obey a time-reversed Schrödinger equation,

$$\frac{d\langle\chi_k(t)|}{dt} = i\langle\chi_k(t)|\hat{H}(t), \tag{22}$$

with the boundary conditions $|\chi_k(T)\rangle = \hat{O}|\Psi_k(T)\rangle$ [29].

The Krotov iterative method is applied to obtain a monotonic growth of the fitness J at each iteration with the correction field,

$$\varepsilon_q^{l+1}(t) = \varepsilon_q^l(t) - \frac{1}{\alpha_q}\sum_{k=1}^{n} \mathrm{Im}\langle\chi_k^l(t)|\hat{\mu}_q|\psi_k^{l+1}(t)\rangle, \tag{23}$$

where $\varepsilon_q^{l+1}(t)$ is the correction for the field after the kth iteration, for the polarization direction q. At each given time step, each field polarization component is modified separately.

Note that the scheme of Eqs. (22) and (23) is somewhat similar to the simultaneous optimization scheme that is needed for unitary transformations and quantum gates. However, for cooling each of the cycles at the final transformation erases the relative quantum phase between the various optimized basis-set initial states. This leaves the resulting fitness measurement at the level of classical transition probability between the initial and final state and removes the need to evaluate quantum phases.

IV. RESULTS

The target of the OCT algorithm is to cool by increasing the purity of the system at the final steady state after multiple cycles. Assuming that the target of the process is to reach a pure, single state, any proposed mechanism for the process [20,30–32] has to maintain the population of the single target state while allowing the population of all other states to repopulate selectively. However, as was shown by [32], the specific choice of the precooling transformation is a subtle issue.

As implied by the ergodic theorem [33], *for any initial state* under multiple cycles of a given field-driven unitary transformation and subsequent decay, the final state will be the invariant under the whole transformation. After many excitation-relaxation cycles, the memory of the initial state will be erased.

Let U be a unitary operator and D be a dissipative operator; there is a stationary state Φ that will obey

$$\lim_{n\to\infty}(U^\dagger DU)^n\phi = \Phi, \tag{24}$$

where ϕ can be any initial state. That is, under a given U and D, the system will finally evolve from any state into the single stationary Φ.

One can obtain the state Φ by diagonalization of the transformation operator $S^\dagger DS$. The stationary state is then given by the eigenstate with a unit eigenvalue, while the next eigenvalue indicates the rate of convergence of the system to the steady state. Using the ergodic theory compels the system to be closed. Since D is fixed, the task is to find the unitary transformation U that will lead to the designed stationary state.

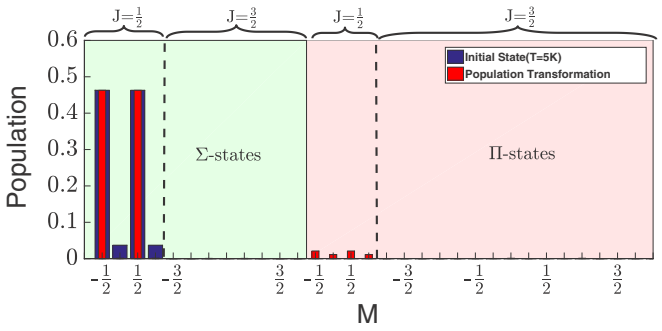

FIG. 2. Starting from $T_{\text{initial}} = 5$ K, the population of the initial thermal states is denoted by the blue bars. After applying the controlled field, the population of the final states at the ground and the excited (red background) electronic states is given by the red bars.

In order to estimate to which extent the system can be controlled by a single field polarized to the Z spatial axis, we start with a restricted problem. Figure 2 displays the initially populated states at temperature of $T \sim 5$ K and the population after a controlled field operation. For this temperature, only the nearly degenerate $J = 1/2$ four-states are populated. The target was to move the population to the excited state at $J = \frac{1}{2}$ and eliminate any transitions to higher-J states that will open decay channels to even higher states. The control field is able to manipulate the system towards the target state with a fitness of 99.9%. However, under a single field that is polarized linearly to the Z direction, no coherent transitions between different M states are allowed. For this example, the final population can be restricted to the lower F_1 states, but the single linearly polarized light cannot break the symmetry between the two M states, limiting the final state that can be reached.

To break the symmetry between different M states, a second perpendicular field is used to control coherent transitions between M states. This addition could be understood as a time-dependent polarization of the field, an experimental control tool that was used for several applications [34,35].

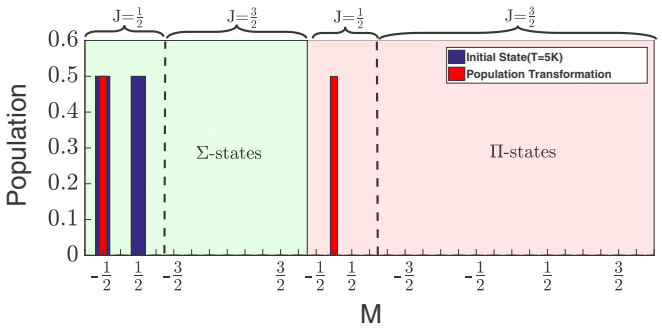

FIG. 3. Breaking the M quantum number degeneracy. Same as Fig. 2, here for the population control of the dual degenerate state (blue) at the ground electronic state (green background) into a nonsymmetric state (red). The target was to maintain the population at one state and excite the population from the other (red background).

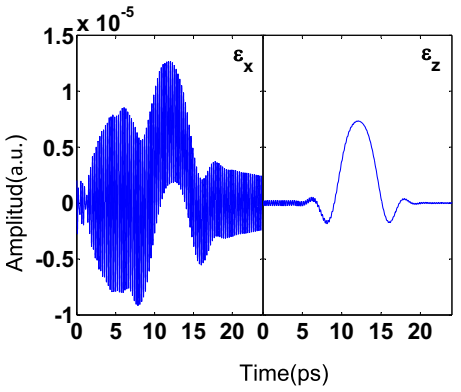

FIG. 4. The two linearly polarized components of the field obtained by the OCT, for the two-state control in the time domain.

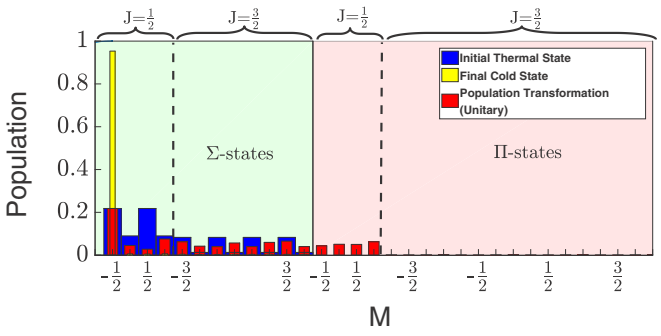

FIG. 6. Subrotational cooling from $T_{\text{initial}} = 20$ K. Similar to Fig. 2, with the final steady state in yellow bars. The final steady state is reached after multiple excitation-dissipation cycles.

Figure 3 shows, by blue bars, the equal thermal population of two degenerate ground states and, by red bars, the population after a controlled field's operation. The target here was to move the $|J = \frac{1}{2}, M = -\frac{1}{2}, F_1\rangle$ population to the excited state at $J = \frac{1}{2}$, while keeping the population at $|J = \frac{1}{2}, M = \frac{1}{2}, F_1\rangle$ unchanged. Figure 4 shows the obtained field components in the Z and X directions as a function of time. The obtained fitness was 99.9%. With such a field, coherent transitions between different M states are allowed and breaking the symmetry between M states was achieved. Nevertheless, such a transformation does not yet lead to cooling due to the fact that the decay of the $J = 1/2$ results in a population in $J = 3/2$ which was not taken into account. We remark here that a single field directed to the X direction can indeed couple states with different M, but the symmetric dynamics for different M states cannot be violated for such a field.

To restrict the system to a closed excitation-relaxation cycle, the control will have to take into account the decay to the ground $J = 3/2$ levels and repump this population to the restricted $J = 1/2$ manifold in the excited state. Figure 5 indicates the desired and eliminated transitions for the control target in the manifold problem.

We chose $|J = \frac{1}{2}, M = -\frac{1}{2}, F_1\rangle$ as the target stationary state of the transformation. The minimal subspace for the optimization has to include the $J = 1/2, 3/2$ manifold; hence, due to the ergodic theorem, the optimization will be able to handle any initial population distribution within these states and lead it to the invariant state. Specifically, a thermal distribution with such occupancy corresponds to an initial temperature of ∼20 K. After excitation, all of the population will be scattered on the Σ states with $(J = \frac{3}{2})$ and only the $J = \frac{1}{2}$ on the excited Π electronic surface.

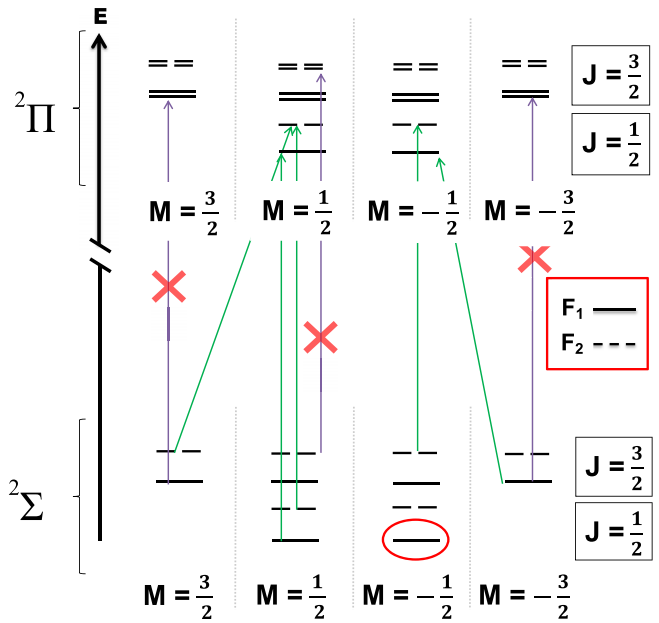

FIG. 5. A schematic description of the cooling mechanism. The control field is able to avoid transformation to $J > 1/2$ in the excited states, and the whole excitation-relaxation cycle is closed. The target state is $|J = \frac{1}{2}, M = -\frac{1}{2}, F_1\rangle$ at the Σ electronic states.

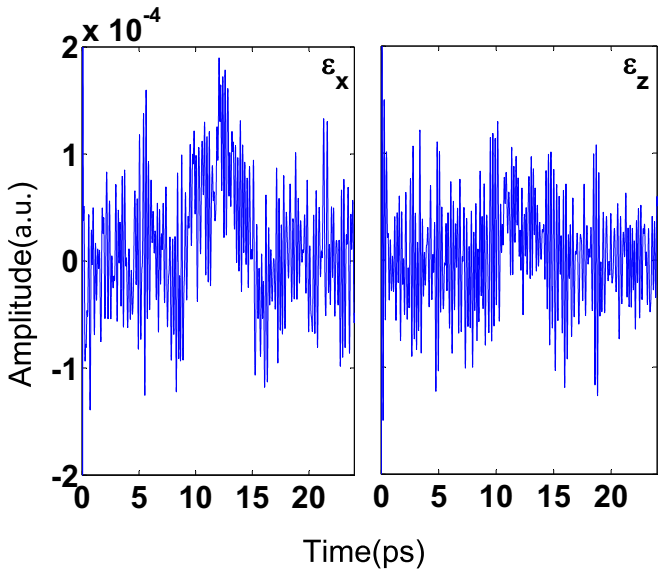

FIG. 7. The field for the subrotational cooling. Similar to Fig. 4, here for the multicycle cooling from $T_{\text{initial}} = 20$ K. Note the significant complex structure of both of the components, in comparison to Fig. 4.

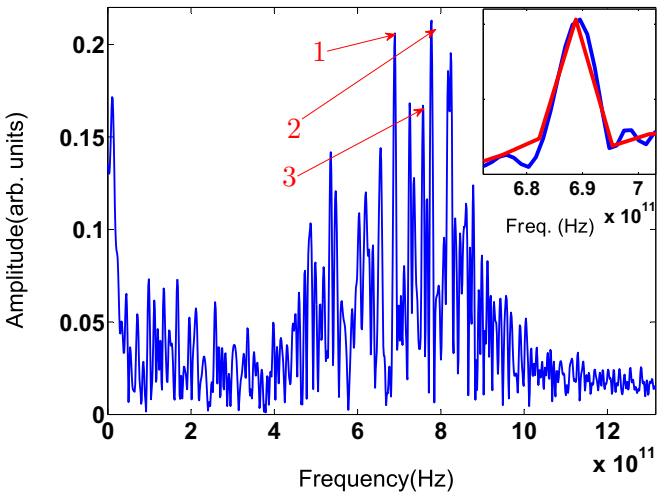

FIG. 8. Frequency domain. Fourier transform of ε_z as a function of the frequency. Three peaks were assigned in the spectrum and correspond to the following allowed transitions: (1) $\langle\frac{1}{2},\frac{1}{2},1|\frac{1}{2},\frac{1}{2},1+\rangle$, (2) $\langle\frac{1}{2},\frac{1}{2},1|\frac{1}{2},\frac{1}{2},1+\rangle$, and (3) $\langle\frac{1}{2},\frac{1}{2},2|\frac{1}{2},\frac{1}{2},2+\rangle$. The time domain was supplemented by zeros to artificially increase the resolution. The inset displays one of the peaks with the original and refined resolutions in red and blue curves, respectively.

Figure 6 shows the results for cooling with the initial thermal state at temperature of $T \sim 20$ K. The blue and red bars are similar to Fig. 2. The yellow bars represent the steady state after multiple excitation-relaxation cycles. The populations at the steady state are not thermally distributed, but are highly concentrated at the single target state, with 95.3% of the population in this single subrotational fine-structure level.

Analysis

Figure 7 presents the obtained highly structured two components of the time-dependent control field.

As expected, the time-domain picture for the field is difficult to encrypt. Some insight could be gained with the inspection of fields in the frequency domain, as shown in Fig. 8. Some of the main peaks in the pulse spectrum can be assigned directly to the energy difference between states in the manifolds (some examples are denoted explicitly).

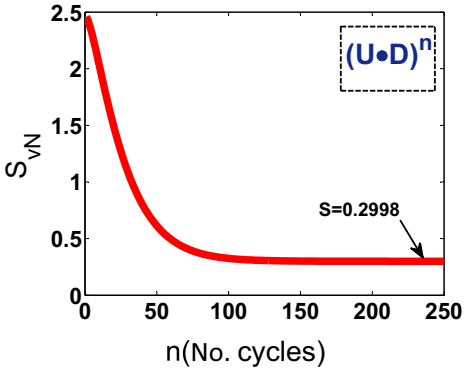

FIG. 9. The von Neumann entropy as defined in Eq. (15) as a function of the number of cycles.

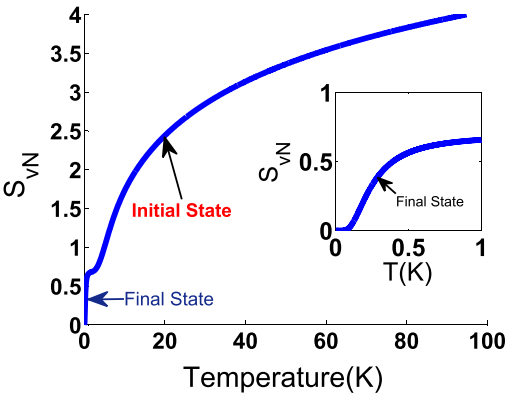

FIG. 10. vN entropy as a function of temperature. The steep slope for $T \to 0$ is magnified at the inset. The abrupt change in the slope reflects the transition in the states occupation from rotational structure into the subrotational structure. The corresponding initial and final states of this work are denoted.

To estimate the temperature of the obtained steady state, we first compute its entropy, as described in Eq. (15). Figure 9 plots the entropy of the state after each excitation-relaxation cycle. A monotonic decrease of the entropy is a clear indication for the cooling of the system. Lindblad has shown that under a completely positive map, the conditional entropy is monotonically decreasing [36].

Figure 10 shows the dependence of the computed vN entropy of the thermal state as a function of the temperature of the system. The curve is then used to calibrate the temperature of any given state. As denoted on the curve, at the initial state the entropy corresponds to a temperature of ∼20 K, while at the final steady state the entropy corresponds to ∼230 mK.

Figure 11 shows the the energy difference between the thermal state and the obtained state after every excitation-relaxation cycle. It is interesting to note that $\Delta\langle E\rangle$ does not decrease monotonically.

At the first cycles, the absorbed energy is greater than the emitted and the excess energy goes to excite the population, while the entropy keeps descending. After ∼10 cycles, $\Delta\langle E\rangle$

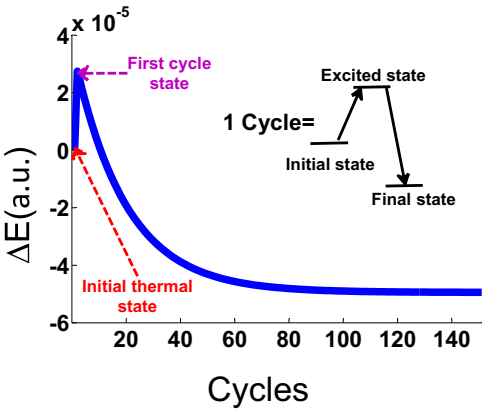

FIG. 11. Energy of the system vs the number of cycles. Note that contrary to Fig. 9, the energy change is nonmonotonic as a function of the number of cycles. $E = 0$ is defined as the energy of the initial thermal state at $T = 20$ K.

starts to converge monotonically, more population resides at lower energy, and $\Delta\langle E\rangle$ decreases.

V. CONCLUSIONS

Cooling molecules using coherent control is an efficient universal method. The light-matter interaction allows energy and entropy transfer between molecules and photons. The mechanism depends on the symmetry of the electronic structure, with insignificant vibrational transitions high FC factors. Our modeling for AlH^+ demonstrates that cooling to the subkelvin regime can be achieved by optimal control (∼230 mK), and can be extended to cool other molecules with a similar electronic structure with almost unity FC factors.

Using two perpendicular linearly polarized light or polarization shaping overcomes symmetry constraints, allowing colder target temperatures.

The mechanisms (energy transfer from the particle to the light medium), used in the ergodic theorem, can be further utilized to find a unitary transformation that will obtain the desired results with higher efficiency [33].

ACKNOWLEDGMENTS

This work is supported by the US-Israel Binational Science Foundation through Grant No. 2012021. This research was supported by the Israel Science Foundation (Grant No. 510/17).

APPENDIX A: THE VIBRATIONAL HAMILTONIAN

For each electronic state, $^2\Sigma$ and $^2\Pi$, we have solved the Schrödinger equation and obtained the eigenvectors and the eigenvalues.

The vibrational Hamiltonian

$$H_{\rm vib} = T + V(r) = \frac{p^2}{2m} + V(r), \tag{A1}$$

where T is the kinetic energy, p is the momentum operator, and V (which depends on r) is the potential-energy operator. We use the Morse potential as the potential-energy operator. It is a convenient interatomic interaction model for the potential energy of a diatomic molecule and accounts for the anharmonicity of real bonds (especially if we are in a low vibrational mode). The Morse potential-energy function is of the form

$$V(r) = D_e(1 - e^{-a(r-r_e)})^2,$$
$$a = \sqrt{k_e/2D_e}. \tag{A2}$$

Here, r is the distance between the atoms, r_e is the equilibrium bond distance, D_e is the well depth (defined relative to the dissociated atoms), and a controls the "width" of the potential. The eigenvalues of the Hamiltonian that was found by solving the Schrödinger equation (which serves as the main diagonal) matches the analytical values,

$$E_{\rm vib} = h\nu_0\left(v + 1/2\right) - \frac{\left[h\nu_0\left(v + 1/2\right)\right]^2}{4D_e}. \tag{A3}$$

The Franck-Condon factors are a multiplicative component of the intensity of electronic transitions between initial and final states of the same or different vibrational number. The FC factors are defined as

$$(\mathrm{FC})_{n,m} = \left|\int \Psi_\Sigma^n \Psi_\Pi^m dR\right|^2, \tag{A4}$$

where Ψ_Σ and Ψ_Π are the vibrational eigenfunctions at each electronic structure.

APPENDIX B: THE ROTATIONAL HAMILTONIAN

In a diatomic molecule, the addition of a second atom breaks the symmetry. In atoms, the motion of the electrons takes place in a spherically symmetric field of force, but this is no longer the case in molecules. The new axis of symmetry is the internuclear axis z. The total angular momentum is

$$J = R + L + S, \tag{B1}$$

where R is the nuclear rotational angular momentum $R = N - L$, L is the electronic orbital angular momentum, S is the electronic spin angular momentum, and N is the total angular momentum excluding electronic spin $N = J - S$. It is important to note that L and S are coupled with the internuclear axis, and the projection on that signed as Λ and Σ, respectively. The projection of the total angular momentum (J) on the molecule axis is

$$\Omega = \Lambda + \Sigma,$$

and the projection on the space fixed axis (Z) is M. Also, the electronic Hamiltonian is invariant under reflections in any plane containing the internuclear axis. If an operator performs a reflection in the molecule-fixed (x,z) plane, then the commutation with the Hamiltonian will be zero. Thus we can conclude that there exist two degenerate eigenfunctions. Since both functions have the same energy, but have some interaction between the rotational motion and the electronic states, it leads to a small splitting in the energy of the two states, which is known as Λ doubling [21].

Hund's cases

We will use Hund's coupling cases to represent the rotational state (at different electronic states). Hund's cases are idealized cases where specific terms appearing in the molecular Hamiltonian and involving couplings between angular momenta are assumed to dominate over all other terms. There are five cases, but most diatomic molecules can be found somewhere between the cases (a) and (b).

Case (a). L is electrostatically coupled to the internuclear axis, and S is coupled to L by spin-orbit coupling. Then both L and S have well-defined axial components Λ and Σ, respectively. Ω defines a vector of magnitude,

$$\Omega = \Lambda + \Sigma,$$

pointing along the internuclear axis. Combined with the rotational angular momentum of the nuclei R, we have

$$J = \Omega + R.$$

In this case, the precession of L and S around the nuclear axis is assumed to be much faster than the rotation of Ω and R

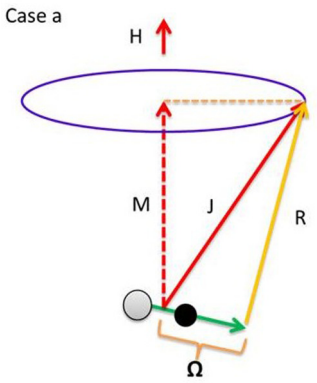

FIG. 12. Hund's case (a).

around J. The good quantum numbers in case (a) are Λ, S, Σ, J, and Ω. The Hund's case (a) coupling scheme is shown schematically in Fig. 12.

Case (b). The spin-orbit coupling is weak or nonexistent (in the case $\Lambda = 0$). In this case, we take

$$J = S + N$$

and assume L precesses quickly around the internuclear axis. Good quantum numbers in this case are Λ, S, N, and J. The Hund's case (b) coupling scheme is shown schematically in Fig. 13. Using these quantum numbers, we can represent any quantum state and any rotational wave function by superposition. For Hund's case (a), the rotational wave function is a symmetric top wave function $|J\Omega M\rangle$. The rotational wave function for a linear molecule (such as the one we use) has only two rotational degrees of freedom and therefore we can write any rotational wave function as [21]

$$|J\Omega M\rangle = \left[\frac{2J+1}{4\pi}\right]^{\frac{1}{2}} D^{J}_{M\Omega}(\phi,\theta,0). \tag{B2}$$

In the $^2\Sigma$, $\Lambda = 0$ (the projection of L on the internuclear axis) and $S = \frac{1}{2}$ (so $\Sigma = \pm\frac{1}{2}$, the projection of S on the internuclear axis), it accounts for Hund's case (a) where L is coupled to the internuclear axis (S is coupled to L). The molecular wave function here is a linear combination of Hund's case (a) wave

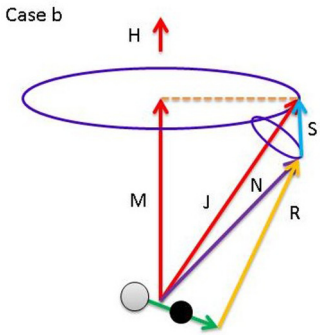

FIG. 13. Hund's case (b).

function and is written as

$$\begin{aligned}|n\Lambda v J\Omega M P^{\pm}\rangle &= \frac{1}{\sqrt{2}}[|n\Lambda\rangle|S\Sigma\rangle|J\Omega M\rangle \\ &\pm|n-\Lambda\rangle|S-\Sigma\rangle|J-\Omega M\rangle]|v\rangle,\end{aligned} \tag{B3}$$

where $P^{\pm}$ denotes the sign of the linear combination and is related to the parity of the wave function. The rotational Hamiltonian for this electronic energy is

$$\begin{aligned}H_{\rm rot}(^2\Sigma) &= B_{(v)}(J-S)^2 + \gamma_v(J-S)S, \\ B_v &= B - \alpha\left(v + {}^1\!/_2\right).\end{aligned} \tag{B4}$$

B is the rotational constant, α is a vibration-rotation interaction constant, and γ_v is the spin-rotation constant.

Solving the Schrödinger equation for this Hamiltonian will give two sets of energy levels corresponding to each parity fragment ($P+$ and $P-$),

$$\begin{aligned}E(^2\Sigma; vJp^+) &= B_v\left(J - {}^1\!/_2\right)\left(J + {}^1\!/_2\right) \\ &\quad + {}^1\!/_2\gamma_v\left(J - {}^1\!/_2\right) \\ &= B_v N(N+1) + {}^1\!/_2\gamma_v N, \\ J &= \frac{1}{2},\frac{3}{2},\frac{5}{2}\cdots, \quad N = 0,1,2,\ldots.\end{aligned} \tag{B5}$$

Those energy levels are for the $P+$ parity block and called F_1 ($J = N + \frac{1}{2}$), and correspond to the $P+$ eigenvector,

$$\begin{aligned}|n\Lambda v J\Omega M P^{+}\rangle &= \frac{1}{\sqrt{2}}[|n\Lambda\rangle|S\Sigma\rangle|J\Omega M\rangle \\ &+|n-\Lambda\rangle|S-\Sigma\rangle|J-\Omega M\rangle]|v\rangle,\end{aligned} \tag{B6}$$

$$\begin{aligned}E(^2\Sigma; vJp^-) &= B_v\left(J + {}^1\!/_2\right)\left(J + {}^3\!/_2\right) \\ &\quad - {}^1\!/_2\gamma_v\left(J + {}^3\!/_2\right) \\ &= B_v N(N+1) - {}^1\!/_2\gamma_v(N+1).\end{aligned} \tag{B7}$$

Those energy levels are for the $P-$ parity block and are called F_2 ($J = N - \frac{1}{2}$), and correspond to the $P-$ eigenvector,

$$\begin{aligned}|n\Lambda v J\Omega M P^{-}\rangle &= \frac{1}{\sqrt{2}}[|n\Lambda\rangle|S\Sigma\rangle|J\Omega M\rangle \\ &-|n-\Lambda\rangle|S-\Sigma\rangle|J-\Omega M\rangle]|v\rangle.\end{aligned} \tag{B8}$$

$^2\Sigma$ energy levels are split by an amount,

$$E(^2\Sigma; vJp^+) - E(^2\Sigma; vJ-1p^-) = \gamma_v J, \tag{B9}$$

in the $^2\Pi$ $\Lambda = \pm 1$ (the projection of L on the internuclear axis) and $S = \frac{1}{2}$ so $\Sigma = \pm\frac{1}{2}$ (the projection of S on the internuclear axis); hence, Ω takes on values $-\frac{3}{2},-\frac{1}{2},\frac{1}{2},\frac{3}{2}$, which accounts to the Hund's cases (a) and (b) where L is coupled to the internuclear axis and S is uncoupled from the nuclear axis. Each $J(M)$ level has four rotational levels associated with it,

two of each parity:

$$\begin{aligned}\left|n^2\pi_{\frac{1}{2}}vJ\Omega MP^{\pm}\right\rangle &= \frac{1}{\sqrt{2}}\left[|n1\rangle\left|\frac{1}{2}-\frac{1}{2}\right\rangle\left|J\frac{1}{2}M\right\rangle\right.\\ &\left.\pm|n-1\rangle\left|\frac{1}{2}\frac{1}{2}\right\rangle\left|J-\frac{1}{2}M\right\rangle\right]|v\rangle,\\ \left|n^2\pi_{\frac{3}{2}}vJ\Omega MP^{\pm}\right\rangle &= \frac{1}{\sqrt{2}}\left[|n1\rangle\left|\frac{1}{2}\frac{1}{2}\right\rangle\left|J\frac{3}{2}M\right\rangle\right.\\ &\left.\pm|n-1\rangle\left|\frac{1}{2}-\frac{1}{2}\right\rangle\left|J-\frac{3}{2}M\right\rangle\right]v\rangle.\end{aligned} \tag{B10}$$

The rotational Hamiltonian for this electronic energy is

$$H_{\rm rot}(^2\Pi) = B_{(r)}[(J-S)-L]^2. \tag{B11}$$

Solving the Schrödinger equation for this Hamiltonian will give two sets of energy levels, where each energy level of a state is the same for each parity block, that is,

$$E(^2\Pi; vJp^+) = E(^2\Pi; vJp^-).$$

Hence they occur in doubly degenerate pairs,

$$\begin{aligned}E(^2\Pi; vJ) &= B_v\left[\left(J-{}^1\!/_2\right)\left(J+{}^3\!/_2\right)\pm{}^1\!/_2X\right],\\ X &= \sqrt{\left[4\left(J-{}^1\!/_2\right)\left(J+{}^3\!/_2\right)+(Y-2)\right]},\\ Y &= \frac{A_v}{B_v},\end{aligned} \tag{B12}$$

where A_v is the spin-orbit interaction constant. The $\pm X$ assigns to the F_1 and F_2 blocks. The energy level associated with the minus sign is called F_1 and corresponds to the eigenvector

$$|\Psi(F_1)\rangle = -b_j\left|^2\pi_{\frac{1}{2}}vJ\right\rangle + a_j\left|^2\pi_{\frac{3}{2}}vJ\right\rangle. \tag{B13}$$

The energy level associated with the plus sign is called F_2 and corresponds to the eigenvector

$$|\Psi(F_2)\rangle = a_j\left|^2\pi_{\frac{1}{2}}vJ\right\rangle + b_j\left|^2\pi_{\frac{3}{2}}vJ\right\rangle, \tag{B14}$$

where

$$a_j = \left[\frac{X+(Y-2)}{2X}\right]^{\frac{1}{2}},\quad b_j = \left[\frac{X-(Y-2)}{2X}\right]^{\frac{1}{2}}, \tag{B15}$$

and F_1 and F_2 represent the magnetic splitting induced by the magnetic interaction between the angular momentum of molecular rotation and the orbital angular momentum, respectively. These Λ-doubled levels are, in turn, split by the coupling of the molecular magnetic moment M, but the difference in the energy of this fine structure is small enough and has been neglected here. We calculated at which J (for the degenerate states) the amount of occupied population is small enough (<0.01) at room temperature. We have found that at 5 K, the population occupies only $J = \frac{1}{2}$ and therefore only four states will be populated. Moreover, we could see that up to 20 K, the population occupies $J = \frac{3}{2}$ states (12 states) and our system size will be dictated by the thermal state that we begin with.

The rotational transition between the two electronic states $^2\Sigma \rightarrow {}^2\Pi$ is dictated by dipole selection rules ($\Delta J = 0, \pm 1$). Transitions with $\Delta J = 0, \pm 1$ denote R, Q, and P (R, Q, P: branches), respectively, and help to assign in which two states the transition occurred. For transitions from F_1 to F_1 and F_2 to F_2, only one subscript is needed [e.g., R_1 transition $^2\Sigma_J(f_1)\rightarrow{}^2\Pi_{J+1}(f_1)$]; all other transitions need two subscripts to define which transition has occurred [$^2\Sigma_J(f_1)\rightarrow{}^2\Pi_{J+1}(f_2)$ is defined by R_{21}]. We have calculated the transitions and assigned them to the right state-to-state transitions.

The nondiagonal elements can be found by calculating the overlap of any two eigenvectors with the dipole operator,

$$\mu_{kl} = \left\langle{}^{\Sigma}\Psi_M^J\left(F_{1,2}\right)\left|\mu\right|{}^{\pi}\Psi_M^{J'}(F_{1,2})\right\rangle. \tag{B16}$$

The only transitions that are allowed are between states with the same M (because the field is linearly polarized and the only transitions are $^2\Sigma \rightarrow {}^2\Pi$ and back).

[1] R. Krems, B. Friedrich, and W. C. Stwalley, *Cold Molecules: Theory, Experiment, Applications* (CRC Press, Boca Raton, FL, 2009).

[2] S. A. Moses, J. P. Covey, M. T. Miecnikowski, D. S. Jin, and J. Ye, New frontiers for quantum gases of polar molecules, Nat. Phys. **13**, 13 (2017).

[3] M. Greiner, C. A. Regal, and D. S. Jin, Emergence of a molecular Bose-Einstein condensate from a Fermi gas, Nature (London) **426**, 537 (2003).

[4] S. Jochim, M. Bartenstein, A. Altmeyer, G. Hendl, S. Riedl, C. Chin, J. H. Denschlag, and R. Grimm, Bose-Einstein condensation of molecules, Science **302**, 2101 (2003).

[5] S. Y. T. van de Meerakker, H. L. Bethlem, N. Vanhaecke, and G. Meijer, Manipulation and control of molecular beams, Chem. Rev. **112**, 4828 (2012).

[6] D. Egorov, T. Lahaye, W. Schöllkopf, B. Friedrich, and J. M. Doyle, Buffer-gas cooling of atomic and molecular beams, Phys. Rev. A **66**, 043401 (2002).

[7] D. J. Larson, J. C. Bergquist, J. J. Bollinger, W. M. Itano, and D. J. Wineland, Sympathetic Cooling of Trapped Ions: A Laser-Cooled Two-Species Non-Neutral Ion Plasma, Phys. Rev. Lett. **57**, 70 (1986).

[8] W. M. Itano, J. C. Bergquist, J. J. Bollinger, and D. J. Wineland, Cooling methods in ion traps, Phys. Scr. **1995**, 106 (1995).

[9] M. Zeppenfeld, B. G. U. Englert, R. Glöckner, A. Prehn, M. Mielenz, C. Sommer, L. D. van Buuren, M. Motsch, and G. Rempe, Sisyphus cooling of electrically trapped polyatomic molecules, Nature (London) **491**, 570 (2012).

[10] F. Masnou-Seeuws and P. Pillet, Formation of ultracold molecules (at 200 μk) via photoassociation in a gas of laser-cooled atoms, Adv. At. Mol. Opt. Phys. **47**, 53 (2001).

[11] N. Proukakis, S. Gardiner, M. Davis, and M. Szymańska, *Quantum Gases: Finite Temperature and Non-Equilibrium Dynamics*, Vol. 1 (World Scientific, Singapore, 2013).
[12] N. Akerman, M. Karpov, Y. Segev, N. Bibelnik, J. Narevicius, and E. Narevicius, Trapping of Molecular Oxygen Together with Lithium Atoms, Phys. Rev. Lett. **119**, 073204 (2017).
[13] A. N. Nikolov, J. R. Ensher, E. E. Eyler, H. Wang, W. C. Stwalley, and P. L. Gould, Efficient Production of Ground-State Potassium Molecules at Sub-mk Temperatures by Two-Step Photoassociation, Phys. Rev. Lett. **84**, 246 (2000).
[14] A. Bartana, R. Kosloff, and D. J. Tannor, Laser cooling of molecules by dynamically trapped states, Chem. Phys. **267**, 195 (2001).
[15] A. Bartana, R. Kosloff, and D. J. Tannor, Laser cooling of molecular internal degrees of freedom by a series of shaped pulses, J. Chem. Phys. **99**, 196 (1993).
[16] A. Bartana, R. Kosloff, and D. J. Tannor, Laser cooling of internal degrees of freedom. II, J. Chem. Phys. **106**, 1435 (1997).
[17] M. Viteau, A. Chotia, M. Allegrini, N. Bouloufa, O. Dulieu, D. Comparat, and P. Pillet, Optical pumping and vibrational cooling of molecules, Science **321**, 232 (2008).
[18] M. Viteau, A. Chotia, M. Allegrini, N. Bouloufa, O. Dulieu, D. Comparat, and P. Pillet, Efficient formation of deeply bound ultracold molecules probed by broadband detection, Phys. Rev. A **79**, 021402 (2009).
[19] M. Hamamda, P. Pillet, H. Lignier, and D. Comparat, Ro-vibrational cooling of molecules and prospects, J. Phys. B **48**, 182001 (2015).
[20] C.-Y. Lien, C. M. Seck, Y.-W. Lin, J. H. V. Nguyen, D. A. Tabor, and B. C. Odom, Broadband optical cooling of molecular rotors from room temperature to the ground state. Nat. Commun. **5**, 4783 (2014).
[21] R. N. Zare, *Angular Momentum: Understanding Spatial Aspects in Chemistry and Physics* (Wiley-Interscience, New York, 2013).
[22] J. V. Neumann, *Mathematical Foundations of Quantum Mechanics*. No. 2 (Princeton University Press, Princeton, NJ, 1955).
[23] A. Lenard, Thermodynamical proof of the Gibbs formula for elementary quantum systems, J. Stat. Phys. **19**, 575 (1978).
[24] D. J. Tannor, *Introduction to Quantum Mechanics* (University Science Books, Herndon VA, 2007).
[25] J. Werschnik and E. K. U. Gross, Quantum optimal control theory, J. Phys. B **40**, R175 (2007).
[26] A. P. Peirce, M. A. Dahleh, and H. Rabitz, Optimal control of quantum-mechanical systems: Existence, numerical approximation, and applications, Phys. Rev. A **37**, 4950 (1988).
[27] R. Kosloff, S. A. Rice, P. Gaspard, S. Tersigni, and D. J. Tannor, Wavepacket dancing: Achieving chemical selectivity by shaping light pulses, Chem. Phys. **139**, 201 (1989).
[28] I. Degani, A. Zanna, L. SÆlen, and R. Nepstad, Quantum control with piecewise constant control functions, SIAM J. Sci. Comput. **31**, 3566 (2009).
[29] J. P. Palao and R. Kosloff, Quantum Computing by an Optimal Control Algorithm for Unitary Transformations, Phys. Rev. Lett. **89**, 188301 (2002).
[30] Y. Maday and G. Turinici, New formulations of monotonically convergent quantum control algorithms, J. Chem. Phys. **118**, 8191 (2003).
[31] R. Eitan, M. Mundt, and D. J. Tannor, Optimal control with accelerated convergence: Combining the krotov and quasi-newton methods, Phys. Rev. A **83**, 053426 (2011).
[32] D. M. Reich and C. P. Koch, Cooling molecular vibrations with shaped laser pulses: Optimal control theory exploiting the timescale separation between coherent excitation and spontaneous emission, New J. Phys. **15**, 125028 (2013).
[33] T. Feldmann and R. Kosloff, Characteristics of the limit cycle of a reciprocating quantum heat engine, Phys. Rev. E **70**, 046110 (2004).
[34] T. Brixner, G. Krampert, T. Pfeifer, R. Selle, G. Gerber, M. Wollenhaupt, O. Graefe, C. Horn, D. Liese, and T. Baumert, Quantum Control by Ultrafast Polarization Shaping, Phys. Rev. Lett. **92**, 208301 (2004).
[35] K. J. Mitchell, N. Radwell, S. Franke-Arnold, M. J. Padgett, and D. B. Phillips, Polarisation structuring of broadband light, Opt. Express **25**, 25079 (2017).
[36] G. Lindblad, Completely positive maps and entropy inequalities, Commun. Math. Phys. **40**, 147 (1975).